Journal of Materials Chemistry B

ROYAL SOCIETY OF CHEMISTRY

PAPER

View Article Online
View Journal

Cite this: DOI: 10.1039/d6tb00666c

Engineering a dual-action nitric oxide and propolis releasing polymeric matrix for extended antimicrobial efficacy

Aasma Sapkota,[a] Sadah Schell,[a] Mofoluwasade O. Popoola,[a] Hitesh Handa [ab] and Elizabeth J. Brisbois *[a]

Received 24th March 2026,
Accepted 29th April 2026

DOI: 10.1039/d6tb00666c

rsc.li/materials-b

Infection of indwelling medical devices is one of the major healthcare threats, often resulting in sepsis, device failure, and even death. The conventional treatment approach for these infections is often systemic, utilizing antibiotics that may lead to unwanted side effects or the development of antibiotic-resistant bacteria. This has led to research into an effective antimicrobial technique that would not further contribute to antimicrobial resistance. Nitric oxide (NO) releasing materials are excellent antimicrobial agents that effectively thwart multiple bacterial strains. Additionally, the incorporation of natural antimicrobial agents such as propolis is a facile and cost-effective way to increase the efficacy and longevity of NO releasing materials without posing any cytotoxic concern. Herein, the fabrication of a NO and propolis releasing polymeric matrix enhanced antimicrobial efficacy against *E. coli*, *S. aureus*, and *C. albicans*. The material was able to release a physiologically relevant amount of NO for 7 days while exhibiting excellent antimicrobial activity through the action of propolis well beyond day 7. The as-reported NO and propolis releasing polymeric substrate showed a significant reduction in the viability of *S. aureus* after incubation under physiological conditions for 28 days, while demonstrating excellent cytocompatibility against 3T3 mouse fibroblast cells. Thus, the reported facile technique for the fabrication of a dual-action antimicrobial polymer can open avenues for their use in indwelling medical device applications.

1. Introduction

According to the US Centers for Disease Control and Prevention (CDC), 1.7 million hospitalized patients acquire healthcare-associated infections (HAIs) annually.[1] On any given day, 1 in 31 patients in hospital acquires an HAI, and this phenomenon is only expected to worsen with the emergence of resistant bacteria.[2] As microorganisms develop resistance, conventional antibiotics lose their effectiveness in treating infections. Thus, the CDC has identified antimicrobial resistance (AMR) as an urgent global threat that requires immediate attention.[3] Resistant bacteria were prevalent even before the discovery of penicillin and have increased exponentially with the excessive use of antibiotics.[4] The global burden of AMR has resulted in a longer duration of illness and a high rate of mortality among patients with resistant infection, in addition to increased cost of treatment.[5]

Antimicrobial resistance is pervasive globally and widely prevalent even in developed countries like the United States. Excess antibiotic prescription is unchecked in the US, as nearly a third of patients who are prescribed antibiotics do not respond to those drugs.[6] Additionally, the use of antibiotics in agriculture to meet high production demands has contributed to increasing AMR.[7] The number of antibiotics discovered and approved in the last decade is limited and falls short of overcoming the multifaceted emergence of resistant bacteria.[8] This issue calls for non-antibiotic-based therapy to treat infections stemming from multiple bacterial and fungal strains without contributing to AMR.

Propolis is a resinous material derived from beehives, consisting of buds, tree sap, pollen, *etc.* Although the exact composition of propolis is dependent on the bee species, location, weather, *etc.*, propolis has been reported to consist of 50% resins and vegetable balm, 30% beeswax, 5% pollen, and 10% essential and aromatic oils.[9,10] It has been used in folk medicine to treat various ailments and has recently gained popularity as a health supplement and a key component in skincare.[11] Recent research has analyzed the potential of propolis in anti-inflammatory, antimicrobial, antiapoptotic, and anti-cancer

[a] *School of Chemical, Materials, & Biomedical Engineering, University of Georgia, Athens, 30602, USA. E-mail: ejbrisbois@uga.edu*
[b] *Pharmaceutical and Biomedical Sciences Department, College of Pharmacy, University of Georgia, Athens, GA, 30602, USA*

applications. Additionally, propolis has shown potential for use in dentistry and treating difficult-to-heal wounds stemming from ulcers or burns.[12]

Incorporating propolis into a polymeric matrix that allows for its controlled release can be an avenue for its inclusion in short-term medical devices. Polymeric medical devices such as catheters can benefit from incorporating antimicrobial agents, as this can increase the life span of these devices and alleviate the risk of infections often associated with catheters. Infections such as central line-associated bloodstream infections (CLABSI) and catheter-associated urinary tract infections (CAUTI) can be treated by using an effective antimicrobial agent like propolis that would not result in resistant bacteria, as is often observed with antibiotic administration.[13] Additionally, antibiotics often target only bacteria, leaving a glaring gap in the effective treatment of fungal infections, which are often overlooked.[14] This demands the fabrication of a non-antibiotic alternative that can be effective against both bacteria and fungi.

In addition to propolis, nitric oxide (NO), a gasotransmitter, can also be incorporated into polymeric medical devices to enhance antimicrobial benefits. Nitric oxide is an endogenous signaling molecule that plays a pivotal role in regulation and host responses throughout the body. The most biologically relevant production of NO happens in the nitric oxide synthase (NOS) family, where mammalian cells produce NO through enzymatic degradation of L-arginine.[15] The physiological NO flux from endothelial cells *via* eNOS is estimated to be 0.5–4 $\times$ 10^{-10} mol min^{-1} cm^{-2}, which is considered the benchmark for NO releasing biomaterial design.[16] On the other hand, macrophages and immune cells express iNOS upon inflammatory stimulation, which generates NO at substantially higher, micromolar-range concentrations, playing a key role in antimicrobial and immune regulatory functions.[17] As NO has a short half-life (a few seconds) and a rapid multi-mechanistic broad-spectrum effect against bacteria, it is biologically improbable for bacteria to mutate and tackle all the oxidative and nitrosative stress stemming from NO.[18] Due to these properties, NO donors are used to deliver NO in a localized manner. Previous reports have shown that NO-based therapies and platforms have incorporated NO donors into gels, ointments, nanoparticles, polymers, coatings, *etc.*[19–21]

Nitric oxide is often incorporated into polymers in the form of NO donor molecules such as *S*-nitrosothiols. Some widely researched *S*-nitrosothiols include *S*-nitrosoglutathione (GSNO) and *S*-nitroso-*N*-acetylpenicillamine (SNAP).[22,23] As a tertiary molecule with enhanced solubility in polar solvents, SNAP is often more desirable for easy incorporation into various medical-grade polymers through swelling or blending.[24] Direct blending of SNAP into a polymeric solution is often desired due to the ease of fabrication and ability to load a higher percentage of SNAP into the polymeric matrix.[21] It is also more stable and has demonstrated long-term NO release and suitability for a wide range of applications. The release of NO from SNAP is achieved through the cleavage of S–NO bonds in the presence of heat, light, metal ions, or enzymes, which opens the avenue for tailored NO release through the incorporation of these catalysts in material design.[25] Although the use of NO releasing surfaces is promising for enhancing the lifetime and cytocompatibility of medical devices, one major issue with NO releasing surfaces is the subsequent loss or degradation of the NO donor within the polymer matrix over time, restricting the antimicrobial ability of the material for a longer duration.[26] Due to this, many recent studies have utilized co-delivery strategies by incorporating bioactive agents in addition to NO donors into the polymeric matrix to extenuate the antimicrobial application of medical devices.[27,28]

Herein, a combinatorial technique for enhancing antimicrobial properties is proposed through the incorporation of an NO donor (SNAP) and propolis into a polymeric matrix of Carbosil, which is a thermoplastic silicone–polycarbonate–urethane widely used in biomedical applications. The material is robust and easy to fabricate, providing an avenue for bulk and large-scale fabrication. The fabricated film possesses the ability to release NO and propolis for local delivery. Additionally, the amount of SNAP leaching out of the sample and NO release through the cleavage of the S–NO bond was evaluated. The fabricated film was tested for its antimicrobial activity against *S. aureus*, *E. coli*, and *C. albicans* to verify the dual-action antimicrobial properties of NO and propolis. The final sample was also tested for long-term antibacterial activity against *S. aureus* after incubation under physiological conditions for up to 28 days. Additionally, all the fabricated samples were tested for their compatibility with mammalian fibroblast cells. Thus, the current dual-action antimicrobial material can be the potential solution to medical device-associated infections without the threat of antimicrobial resistance.

2. Experimental

2.1 Materials

N-Acetylpenicillamine (NAP), tetrahydrofuran (THF), sodium nitrite ($NaNO_2$), ethylenediaminetetraacetic acid (EDTA), hydrochloric acid (HCl), sulfuric acid (H_2SO_4), and MTT (3-[4,5-dimethylthiazol-2-yl]-2,5-diphenyl tetrazolium bromide) were purchased from Sigma-Aldrich (St. Louis, MO 63103). Carbo-Sil™ 2080A (Carbosil) was obtained from DSM Biomedical Inc. (Berkeley, CA). Dulbecco's modified Eagle's medium (DMEM) and trypsin-EDTA were purchased from Corning (Manassas, VA 20109). Penicillin–streptomycin (Pen-Strep) and fetal bovine serum (FBS) were obtained from Gibco-Life Technologies (Grand Island, NY 14072). Drabkin's reagent was purchased from VWR (Atlanta, GA). The bacterial strains *Staphylococcus aureus* (*S. aureus* ATCC 6538), *Escherichia coli* (*E. coli* ATCC 25922), *Candida albicans* (*C. albicans* MYA 4441), and NIH/3T3 mouse fibroblast cells were purchased from American Type Culture Collection (ATCC). Phosphate-buffered saline (PBS), 0.01 M, pH 7.4 (confirmed with a Mettler Toledo pH meter), used for *in vitro* experiments, containing 138 mM NaCl, 2.7 mM KCl, and 10 mM sodium phosphate, was purchased from Sigma-Aldrich (St. Louis, MO 63103). Luria–Bertani (LB) broth and yeast extract peptone dextrose (YPD) were obtained from

Fisher Bioreagents (Fair Lawn, NJ). LB Agar and YPD agar were purchased from Difco Laboratories Inc. (Detroit, MI). All the buffers and media were sterilized in an autoclave at 121 °C, 100 kPa (15 psi above atmospheric pressure) for 30 min before biological studies.

2.2 Fabrication of the samples

2.2.1. Synthesis of *S*-nitroso-*N*-acetylpenicillamine. *S*-Nitroso-*N*-acetylpenicillamine (SNAP) was synthesized by modifying a previously established protocol.[29] Briefly, 5 g *N*-acetylpenicillamine (NAP) was dissolved in 60 mL of methanol to which 5 mL of concentrated HCl and 20 mL of H_2SO_4 were added. After successful dissolution of NAP, 5 g of $NaNO_2$ dissolved in 40 mL DI water was added dropwise to the mixture to nitrosate the solution. This solution was protected from light and placed in an ice bath for 8 h to allow for precipitation of SNAP crystals. Finally, SNAP crystals were collected by vacuum filtration, and unreacted nitrites were removed by washing the product with DI water. The product was then dried overnight in a desiccator to remove any trace solvent and stored at −20 °C in the dark until further use.

2.2.2. Nuclear magnetic resonance. The purity of the synthesized SNAP was determined using a ^{1}H NMR Bruker Ascend 400 MHz spectrometer. First, SNAP was dissolved in dimethyl sulfate-d6 (DMSO-d6) and analyzed by NMR. The purity was analyzed through the integration of the peak obtained from the spectra.

The purity of SNAP was estimated by ^{1}H NMR using NAP (purity >99%) as an internal standard. NAP (10.0 mg, MW 191.25 g mol^{-1}) and SNAP (24.0 mg, MW 220.2 g mol^{-1}) were dissolved in DMSO-d6 and analyzed by ^{1}H NMR. Integrations of the acetyl methyl resonances were used for quantification (NAP: δ 1.92 ppm, 3H; SNAP: δ 1.88 ppm, 3H).

2.2.3. Fabrication of films. Polymer films were fabricated by casting polymer solutions in a Teflon mold. Carbosil pellets (70 mg mL^{-1}) were dissolved in THF dried using 3A molecular sieves (20 w/v%), cast into a Teflon mold, and allowed to dry overnight in a fume hood. Additionally, the films were dried in a desiccator for 24 h to remove any trace solvents. For propolis films, 1 wt%, 3 wt%, or 5 wt% propolis was added to the polymer solution. Similarly, for S films, 10 wt% SNAP was added to the polymer solution before casting the film. Finally, SNAP–propolis films were prepared by adding the required wt% of propolis and 10 wt% SNAP to the polymer solution. For all the experiments, a 6 mm disk out of the film was punched out using a hole puncher, which resulted in polymer films with a thickness of ∼0.24 cm, resulting in a surface area of ∼1 cm^2.

2.3 Film characterization

2.3.1. Contact angle measurement. The static contact angle of the fabricated films was measured using a contact angle goniometer (Ossila, Sheffield, UK). A 5 μL droplet of deionized water was deposited on the surface, and the contact angle was calculated by Ossila Contact Angle software using the sessile drop approximation.

2.3.2. Mechanical testing. The effect of SNAP and/or propolis on the polymer's Young modulus was investigated by subjecting the samples to mechanical testing on a Mark-10 ESM303 motorized test stand. The sample for testing was punched out to dog bone shapes using the ASTM D-1708 Specimen Die (Pioneer-Dietecs, MA), and the dimensions of the sample (gauge length, gauge width, and sample thickness) were recorded prior to testing. Samples were subject to a speed of 10.1 mm min^{-1}. The resulting force–displacement curve was converted to a stress–strain curve using eqn (1) and (2). The slope of the linear region of the stress–strain curve provided the Young's modulus, shown by eqn (3) ($n \geq 8$).

$$\text{Stress} = \frac{\text{force}}{\text{cross-sectional area}} = \frac{\text{force}}{\text{gauge width} \times \text{sample thickness}} \quad (1)$$

$$\text{Strain} = \frac{\text{change in length}}{\text{original length}} = \frac{\text{displacement}}{\text{gauge length}} \quad (2)$$

$$\text{Young's modulus} = \frac{\text{stress}}{\text{strain}} \quad (3)$$

2.4 NO release kinetics

The NO release from different film samples was measured using a Sievers chemiluminescence nitric oxide analyzer (NOA 280i, Zysense, Boulder, CO, USA). The samples were introduced in an amber reaction chamber containing PBS with 100 μM EDTA, which chelates any catalytic NO release from the presence of metals. The NO release was quantified by submerging the reaction chamber in a water bath at 37 °C. The chamber was continuously purged with nitrogen gas at the rate of 200 mL min^{-1} to help purge the produced NO from the solution and to stabilize the free radical. The NO produced from the reaction then reacts with ozone to produce nitrogen dioxide in an excited state (NO^{2*}), which decays to produce a photon, which is detected by a photomultiplier tube (PMT) to calculate the amount of NO being released from the sample in ppb. The measured NO release is converted to flux values using the NOA constant and normalized to the total surface area of the samples.

2.5 Leaching and loading

SNAP and propolis leaching studies were conducted over 28 d under physiological conditions in PBS. The leaching was quantified by reading the absorbance of the solution at different time points using a UV-vis spectrophotometer (Cary 60, Agilent Technologies). The absorbance value corresponding to 275 nm was recorded for propolis, and the absorbance value corresponding to 340 nm was recorded for SNAP. The molar absorptivity of SNAP in 10 mM PBS at pH 7.4 was determined to be 1053 M^{-1} cm^{-1} at the wavelength of 340 nm. The absorbance value was converted to concentration in mg cm^{-2} by using a standard calibration curve of SNAP and propolis. Additionally, SNAP loading was determined by incubating the samples in methanol for 3 h and then reading the absorbance of the methanol solution.

2.6 *In vitro* antimicrobial activity

2.6.1. Preparation of bacterial culture. Single isolated colonies of bacterial strains: *E. coli* and *S. aureus* were inoculated in LB broth, whereas *C. albicans* was inoculated in YMA broth and incubated at 37 °C for 8 h at 150 rpm. The bacterial culture was centrifuged at 3500 rpm for 7 min to isolate a bacterial pellet before re-suspending the pellet in PBS solution (pH 7.4). The bacterial solution was then diluted to obtain an optical density (OD) of 0.1 using a UV-vis spectrophotometer (Cary 60, Agilent Technologies) at a wavelength of 600 nm, yielding a final bacterial concentration of $\sim 10^6$ colony-forming units (CFU) mL^{-1}.

2.6.2. Quantification of planktonic bacteria. To determine the efficacy of the samples against bacteria, a 0.6 cm diameter film with a surface area of *ca.* 1 cm^2 was fabricated and sterilized under UV light for 30 min. Afterward, the samples were incubated in 1 mL of diluted bacterial solution for 24 h while shaking at 150 rpm. Next, the bacterial solution was diluted and plated onto LB agar plates for *E. coli* and *S. aureus* and YMA agar plates for *C. albicans* using a spiral plater (Eddy Jet 2, IUL Instruments). The agar plates were incubated at 37 °C for 24 h, after which the bacterial colonies on the agar plates were counted using an automated colony counter (Sphere Flash, IUL Instruments). The CFUs of planktonic bacteria were quantified and normalized to the surface area. The percentage of reduction in bacterial viability was determined by eqn (4) (with respect to Carbosil control), where C represents the concentration of viable bacteria in CFU:

$$\%\ \text{reduction} = \frac{C(\text{control}) - C(\text{test group})}{C(\text{control})} \times 100 \qquad (4)$$

2.6.3. Quantification of adhered bacteria. For further antimicrobial analysis of the films, the number of adhered *E. coli*, *S. aureus*, and *C. albicans* on the film samples was determined following a similar exposure technique as in section 2.6.2. After 24 h of incubation at 37 °C, the films were retrieved and washed with PBS to remove loosely adhered bacteria. Then, the samples were homogenized at 25 000 rpm using an Omni-TH homogenizer (Omni, Kennesaw, GA) for 1 min, followed by 1 min vortexing to extract all the adhered bacteria into PBS solution. This solution was then diluted and plated on respective agar plates using a spiral plater (Eddy Jet 2, IUL Instruments) and counted the next day after incubation at 37 °C using an automated colony counter (Sphere Flash, IUL Instruments). The percentage reduction of adhered bacteria was calculated using the same equation as in section 2.6.1.

2.6.4. Long-term antibacterial assay. The efficacy of the fabricated samples against *S. aureus* after incubation in PBS was determined by quantifying the adhered and planktonic bacteria. Film samples with an area of ~ 1 cm^2 were incubated in PBS for 7, 14, or 28 days. After incubation, the samples were retrieved, UV sterilized, and tested against *S. aureus* through a 24 h antibacterial assay following sections 2.6.1–2.6.3.

2.7. *In vitro* cytotoxicity assay

2.7.1. Leachate based cytocompatibility. The biocompatibility of the fabricated samples was assessed using a leachate-based MTT assay. For leachate preparation, the samples were UV sterilized and incubated in 1 mL of complete DMEM (DMEM + 10% FBS + 1% PS) for 24 h at 37 °C. For cell growth, a cell culture treated 96-well plate was seeded with 3T3 mouse fibroblast cells (5000 cells per well) and the plate was incubated at 37 °C for 24 h with 5% CO_2. The next day, the leachates obtained from the samples were added to the cell-seeded well plate following the ISO standards (ISO10993-5:2009 Test for *in vitro* cytotoxicity assessment of biomedical devices). The leachate interacted with the cells for 24 h at 37 °C with 5% CO_2. Afterward, the media were pipetted out from the well plate, and 10 μL of MTT solution (5 mg mL^{-1}) and 90 μL of PBS were added to each well, and the plate was incubated at 37 °C for 3 h. After incubation, the MTT + PBS solution was pipetted out and 100 μL of DMSO was added to each well to dissolve formazan crystals through gentle rocking. The formation of formazan crystals reduced from MTT by viable cells was visualized by a distinct color change and then quantified using a plate reader (Cytation 5 imaging multi-mode reader, BioTek). The absorbance (A) of the wells at 570 nm is reported in terms of relative cell viability compared to the control cells.

$$\text{Cell viability} = \frac{A(\text{test group})}{A(\text{control})} \times 100\% \qquad (5)$$

2.7.2. Indirect contact cytocompatibility. The indirect contact cytocompatibility was assessed by seeding a cell culture-treated 24-well plate with 3T3 mouse fibroblast cells (10 000 cells per well) and allowing the plate to incubate for 24 h at 37 °C with 5% CO_2. After incubation, UV-sterilized samples were introduced into the wells using a *trans* well, after which the plate was incubated again under the same conditions for another 24 h. The next day, the MTT assay was performed following the same steps and calculation as in section 2.7.1.

2.8 Hemolysis

The potential hemolytic response of the fabricated samples was tested against porcine blood. The porcine blood was diluted with calcium and magnesium-free PBS (CMF-PBS) to a total hemoglobin concentration of 10 ± 1.0 mg mL^{-1}. Next, the blood was diluted with either sterilized deionized water for positive control or CMF-PBS as a blank at a concentration of 1 : 7. The fabricated samples were incubated in dilute whole blood at 37 °C for 3 h with manual rocking every 30 min. After incubation, the samples were centrifuged at 800 g for 15 min, and the supernatant was collected. This supernatant was then combined with a 1 : 1 ratio of Drabkin's reagent and allowed to incubate for 15 min at room temperature. The absorbance was then read at 540 nm and the hemolysis was quantified as a percentage value.

2.9 Statistical analysis

All experiments in this study are conducted with a sample size of $n \geq 4$. Data are reported as mean ± standard deviation (SD).

All statistical analyses were performed using Prism 10 (GraphPad Software, San Diego, CA). Statistical comparisons of treatment groups against control groups were analyzed using one-way ANOVA with Tukey's method for correcting multiple comparisons. Bacterial statistical analysis was performed on the log values of CFUs for each treatment. Values of $p < 0.05$ were deemed statistically significant.

3. Results and discussion

3.1 Fabrication and characterization of samples

The NO donor SNAP and propolis were integrated into the polymeric matrix through a facile blending method where the compounds were incorporated into the polymeric solution before casting it into a thin film (Fig. 1C). SNAP is a well-documented NO donor that has been incorporated into various medical-grade polymeric materials such as polyurethane, polyvinyl chloride, silicone rubber, *etc.*, through blending, swelling, and covalent bonding (Fig. 1B).[30,31] Additionally, propolis contains various functional groups such as alkaloid, flavonoid, terpenoid, *etc.* that can exert antimicrobial properties through a wide range of bacterial pathways (Fig. 1A).[32] While this enhanced biological property has made propolis attractive for a wide range of applications, the complex chemical composition sometimes presents itself as an obstacle for broader use of propolis in the pharmaceutical industry due to the issue of standardization.[33] Several approaches towards standardization of propolis, such as chemical marker identification of bioactive constituents, high-performance liquid chromatography for profiling of propolis, implementation of a standardized process of propolis extraction, blending of raw materials, and botanical and geographical classification of propolis, have been established for the commercialization of propolis.[34] This has led to the extension of the application of propolis releasing materials in wound healing, food packaging, *etc.*[35,36] Hence, the incorporation of these two bioactive agents can provide an avenue for fabricating a synergistic material for medical device applications.

The effect of incorporating SNAP and propolis in the polymeric matrix was analyzed by investigating the surface wettability of the fabricated film samples. The change in surface properties of the films through the incorporation of 1 wt%, 3 wt%, and 5 wt% propolis was determined through the analysis of the surface contact angle. 5 wt% was chosen as the maximum saturation point of propolis, as concentrations beyond 5 wt% resulted in the formation of non-homogeneous films. Additionally, 10 wt% SNAP was incorporated into the film following previous reports.[37,38] The water contact angle recorded on the surface of the films with different concentrations of propolis and 10 wt% SNAP showed no significant change in surface hydrophobicity (Fig. 1D). This shows that the incorporation of these compounds does not affect the surface properties of the material and retains hydrophobicity with a contact angle of >90. Hydrophobic materials are often desired for biomedical applications as they can reduce biofouling through the reduction of protein and biofilm adhesion to the surface of implantable medical devices.[39]

3.2 Investigation of mechanical properties

The mechanical properties of implantable medical devices are critically important, as for successful implantation and longevity, the fabricated polymer should closely match the structural and

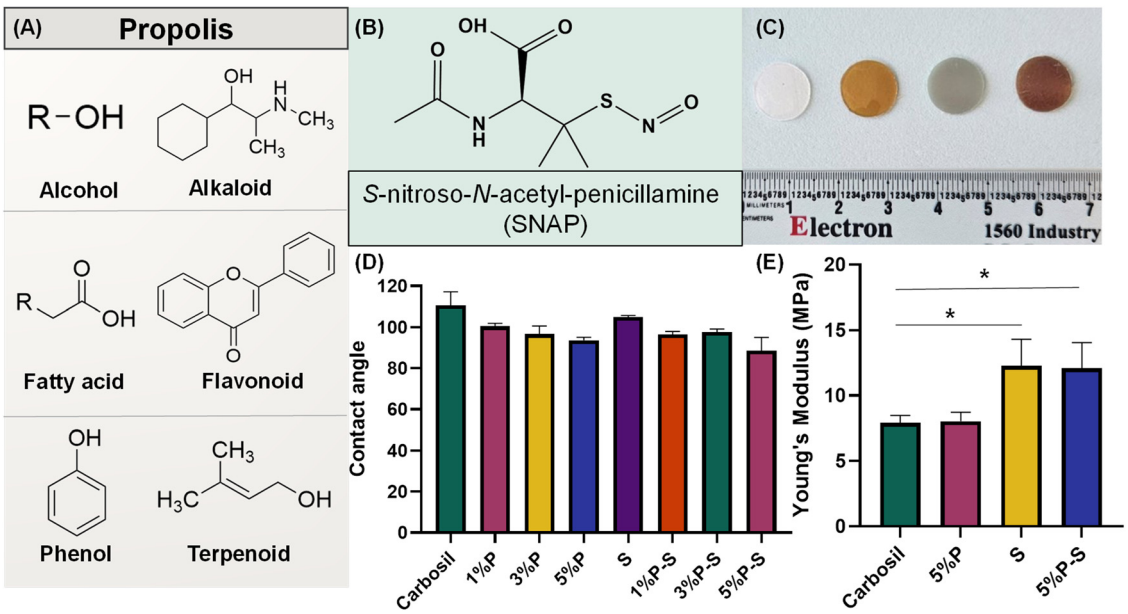

Fig. 1 (A) Major functional groups present in propolis for exerting biological applications. (B) Chemical structure of the NO donor SNAP. (C) Fabricated films: Carbosil, 5% P, S, and 5% P–S (left to right). (D) Water contact angles of various fabricated films. (E) Mechanical properties of the films assessed using Young's modulus. Comparisons against control values are performed using one-way ANOVA with Tukey's method. * represents $p \leq 0.05$. All data are presented as mean ± SD ($n \geq 4$).

functional characteristics of native tissue. Additionally, the incorporation of bioactive components should not diminish the native mechanical features of the polymer.[40] Here, mechanical testing was performed to investigate the effect of SNAP and/or propolis on the stiffness of the final material. For unmodified Carbosil, Young's modulus was found to be 7.909 ± 0.5698 MPa. Similarly, the addition of propolis to Carbosil (5%P) gave the polymer a Young's modulus of 8.022 ± 0.7077 MPa, showing that the addition of propolis had no significant effect on the mechanical behavior of the polymer. However, with the addition of SNAP to the polymer, there was a significant increase in Young's modulus by nearly half, resulting in a stiffer material. For the SNAP blended Carbosil (S) sample, the Young's modulus was 12.27 ± 2.038 MPa, while samples containing both SNAP and propolis (5%P–S) provided a Young's modulus of 12.10 ± 1.95 MPa (Fig. 1E). It can be inferred that the increase in Young's modulus is due to the presence of crystallized SNAP within the blended polymer, with no effect of propolis on the mechanical properties of the polymer, as there was no significant change in the Young's modulus of 5%P–S when compared to S.[41]

There have been several reports of biomaterials that show a similar trend of increasing Young's modulus due to the addition of crystalline molecules (*e.g.* drugs), as the crystals can reinforce the polymer system and make the final material stiffer.[42,43] Previous studies have shown that when SNAP is incorporated into a hydrophobic polymeric matrix, it can exist in both dissolved and crystalline phases due to its intermolecular interactions and limited solubility.[44] The presence of these crystalline structures can act as rigid dispersed phases within the softer polymeric matrix of Carbosil. Additionally, the increase in stiffness or Young's modulus can be linked to the presence of crystalline domains as these rigid components restrict the polymer chain mobility and enhance the resistance of the material to elastic deformation. SNAP crystallization within the hydrophobic polymer matrix can also be associated with intermolecular hydrogen bonding which further reduces the mobility of polymer chains.[45] The presence of SNAP crystals in the sample is often preferable as it facilitates the stability of the NO donor and extends the release profile.[46]

3.3 Analysis of NO release kinetics

With their potential for tailored NO release from various polymeric matrices, RSNOs such as SNAP and GSNO have been extensively explored. SNAP is a synthetic tertiary RSNO formulated from the amino acid penicillamine, whereas GSNO is a primary RSNO that is endogenously produced and often desired for its bioavailability.[47,48] Water-soluble GSNO is usually the NO donor of choice for aqueous systems like hydrogel, but is often found to be difficult to incorporate in non-aqueous systems.[49] With excellent solubility in polar solvents such as THF and potential for long-term NO release and subsequent bioactivity, SNAP has been the NO donor of choice for various *in vivo* experiments.[50–52] It is important for NO release to be tailored for application in the human body while mitigating the risk of toxicity from burst release, as the physiological level of NO release is estimated to be 0.5–4 × 10^{-10} mol min^{-1} cm^{-2}.[16] The purity of the synthesized SNAP in this study was found to be 96.4% through comparison of spectra for NAP and SNAP (Fig. S5 and S6).

S-Nitrosothiols like SNAP can release NO through the cleavage of the S–NO bond in the presence of heat, light, or metal ions.[53] The amount of NO release from the polymer film can be quantified in real-time using chemiluminescence NOA at 37 °C, as shown in Fig. 2A. The analysis through NOA showed a physiologically relevant amount of NO release with all sample types, demonstrating no change in NO release kinetics through the incorporation of propolis. On day 0, NO release from S, 1%P–S, 3%P–S, and 5%P–S samples was found to be 1.12 ± 0.17, 1.00 ± 0.21, 1.19 ± 0.23, and 1.32 ± 0.17 × 10^{-10} mol cm^{-2} min^{-1}, respectively. A similar NO release trend continued over 7 days, with NO release between 0.11–0.21 × 10^{-10} mol cm^{-2} min^{-1} on day 7 (Fig. 2B). The NO release study was conducted for 7 days since the NO release level on day 7 demonstrated sub-endothelial levels of NO release. As the amount of propolis loaded did not affect the NO release behavior, the film with the maximum amount of propolis, *i.e.*, 5%P–S, was selected for further biological study to exert maximum antimicrobial efficacy of propolis. Additionally, similar levels of NO release as seen in this NO release experiment have shown excellent antimicrobial activity in the past.[26,54]

3.4 Analysis of SNAP and propolis leaching

In addition to ensuring an optimal level of NO release, it is also crucial for effective biomaterials to have minimal leaching of loaded active components. Excessive leaching of SNAP or propolis can result in undesirable side effects or cytotoxicity. To quantify the concentration of leachate solution, a standard curve was prepared for both SNAP and propolis solution (Fig. S2 and S4). With propolis, a steady amount of propolis leaching was observed, which is desirable for a long-term antimicrobial application. On day 1, ~0.06 mg cm^{-2} of propolis leached out of 5%P and 5%P–S samples. A similar propolis leaching pattern was observed with 5%P and 5%P–S samples throughout the experiment, with cumulative propolis leaching ~0.23 and ~0.26 mg cm^{-2} (15.33% and 17.33% of loaded propolis), respectively, on day 28 (Fig. 2C). On the other hand, minimal SNAP leaching was observed with S and 5%P–S samples, as ~0.12 mg cm^{-2} (4% of loaded SNAP) of SNAP was found to have leached out of the samples (Fig. 2D). A slightly lower SNAP leaching from 5%P–S samples when compared to S during initial time points can be attributed to the incorporation of propolis, which could alter the internal microstructure of the polymeric matrix. This can reduce the free volume of SNAP by increasing intermolecular interactions and thereby hindering SNAP diffusion as hydrophobic inclusions like propolis can hinder/slow drug release.[55]

Materials with similar SNAP leaching patterns have shown excellent antimicrobial properties with no leaching-associated cytotoxicity concerns, as most of the SNAP reservoir is diffused in the form of NO.[56] Additionally, the propolis leaching amount observed here lies within the reported MIC value of the ethanolic extract of propolis, which has been reported to be

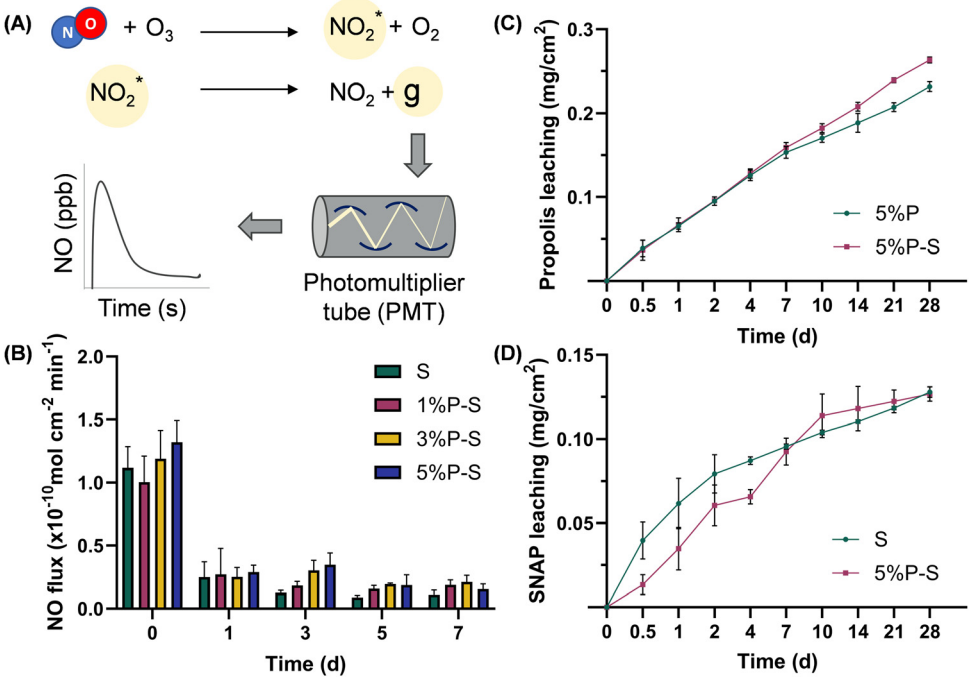

Fig. 2 (A) Schematic of the reaction between NO and O_3 for the production of excited NO_2 which is later transformed into excited photons and quantified by using a photomultiplier tube. Yellow circles track the conversion of excited NO_2 to a numerical value. *g* represents a photon. (B) NO release from S, 1%P–S, 3%P–S, and 5%P–S samples over 7 days under physiological conditions. Leaching of (C) propolis and (D) SNAP from film samples quantified by reading absorbance on a UV-vis spectrophotometer over 28 days. All data are presented as mean ± SD ($n \geq 4$).

~710–1420 μg mL^{-1}.[57] Although the bioactivity of propolis differs highly based on numerous environmental factors, most reports suggest that the obtained concentration of propolis leachate should elicit significant antimicrobial activity.[58]

3.5 Investigating the antimicrobial activity of NO and propolis

Medical devices such as catheters are susceptible to bacterial colonization when introduced into the body, leading to shortened device life span and ultimately device failure. Catheter-related infections can stem from many sources, including the skin flora, contaminated catheter hub, and contaminated infusate.[59] In addition to the multiplicity of sources of infection, antimicrobial resistance often renders systemic antibiotics unable to treat these nosocomial infections, compromising patients' safety and well-being.[60] Addressing bacterial colonization to extend the life span of medical devices without contributing to the ever-increasing threat of antimicrobial resistance can be the solution to increased healthcare costs and the evolution of superbugs.

The use of non-antibiotic antimicrobial agents, such as NO donors or natural antimicrobial components, such as propolis, can help overcome the challenges of antimicrobial resistance. In the past, NO releasing materials have shown antibacterial activity against Gram-positive, Gram-negative, and resistant bacterial strains.[61] Additionally, propolis has been extensively studied for its bioactivity and health benefits, including antibacterial and antifungal properties.[62] The local delivery of natural agents like NO and propolis helps alleviate the concern of associated toxicity often observed with oral administration of antibiotics. Hence, the current work explores the complementary antimicrobial efficacy of NO and propolis releasing polymer to tackle the ever-growing threat of nosocomial infection (Fig. 3A).

The antimicrobial activity of the fabricated samples was assessed by exposing the samples to various bacterial solutions under physiological conditions and counting CFUs of adhered and planktonic bacteria. For this study, four sample types, Carbosil, 5%P, S, and 5%P–S, were exposed to Gram-positive *S. aureus*, Gram-negative *E. coli*, and a fungal strain of *C. albicans*. Upon exposure to *C. albicans*, 5%P and S controls showed antifungal activity with 56.84% and 75.24% reduction in adhered fungal strains, whereas the test group 5%P–S showed 96.69% reduction. A similar reduction trend was observed in the planktonic *C. albicans* experiment with an 88.84% reduction from 5%P–S (Fig. 3B). In the case of adhered *E. coli*, 86.63%, 90.18%, and 97.16% reduction was seen with 5%P, S, and 5%P–S, respectively, along with 94.74% reduction in planktonic *E. coli* with the 5%P–S group (Fig. 3C). Finally, with *S. aureus*, 5%P, S, and 5%P–S samples showed 98.23%, 98.19%, and 99.93% reduction in viability of adhered bacteria. Additionally, a 99.49% reduction in the viability of planktonic *S. aureus* was observed (Fig. 3D). The antimicrobial pattern seen with the 5%P–S sample agrees with other reports of antimicrobial activity reported with the NO releasing matrix and ethanolic extract of propolis.[63,64]

The antimicrobial properties of NO against a wide range of microbes can be attributed to its reactivity and formation of reactive byproducts that cause oxidative and nitrosative stress.[65]

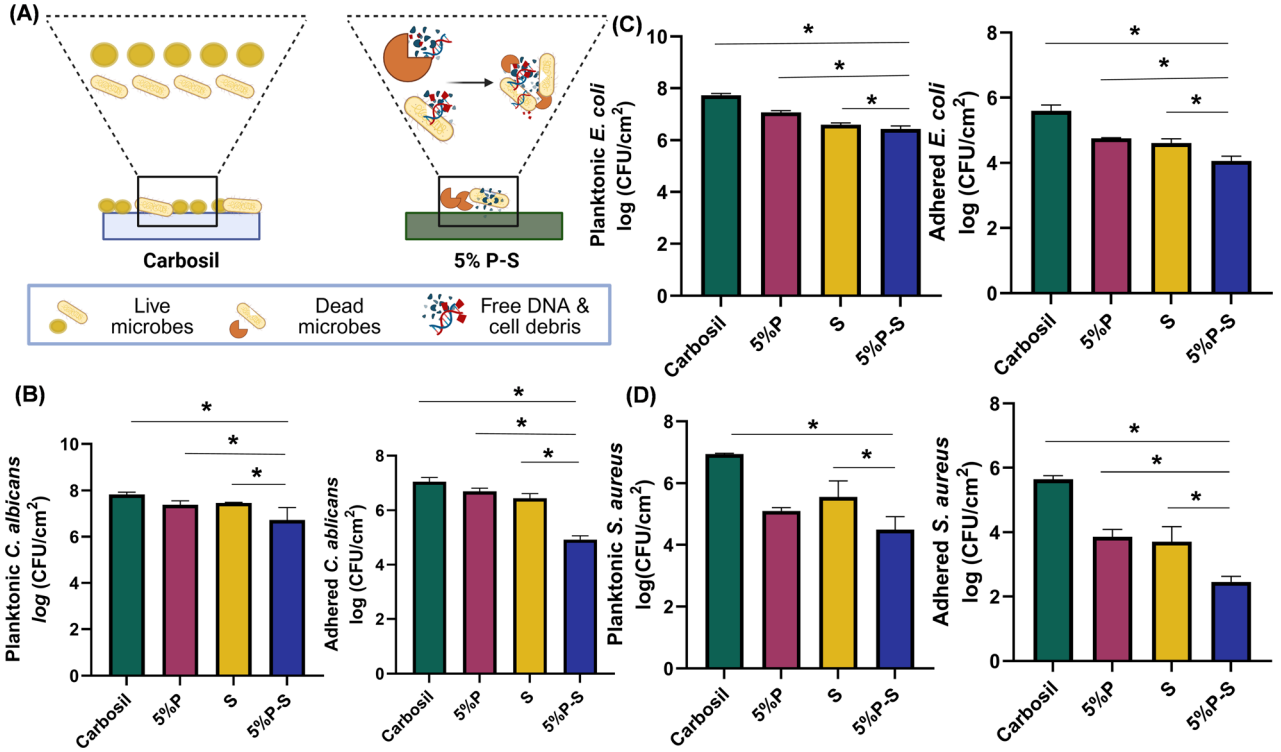

Fig. 3 Antimicrobial activity of film samples against *E. coli*, *S. aureus*, and *C. albicans*. (A) Schematic of antimicrobial activity of NO and propolis releasing films. (B) Reduction in planktonic and adhered CFU cm^{-2} of (B) *C. albicans*, (C) *E. coli* and (D) *S. aureus*, with the dual action of NO and propolis releasing films. Comparisons against control values were performed using one-way ANOVA with Tukey's method. * represents $p \leq 0.05$. All data are presented as mean ± SD ($n \geq 4$).

The main mechanism of NO mediated antimicrobial action is through chemical alteration of DNA by RNOS which inhibits the ability of bacterial DNA to repair itself in addition to increased generation of genotoxic alkylating agents and hydrogen peroxide.[18] However, multiple converging interactions and mechanisms contribute towards the overall antimicrobial activity *via* oxidative and nitrosative stress. The diffusion limited interaction of NO with the superoxide radical (O_2^-) (generated by bacteria under metabolic stress) leads to the formation of peroxynitrite ($ONOO^-$), which is a potent and short lived oxidant.[66] In addition to peroxynitrite mediated damage, NO can bind to iron in iron–sulfur cluster proteins (Fe–S) to form dinitrosyl iron complexes (DNICs), which inhibits central metabolic enzymes and components of the bacterial electron transport chain.[67] All of these mechanisms collectively disrupt bacterial energy metabolism, DNA integrity, and membrane function, contributing towards the broad-spectrum antimicrobial action of NO.

Additionally, propolis has its own bacteriolysis mechanism comprising numerous pathways. The active components in propolis can attach to the cytoplasmic membrane of the bacterial cell, causing perforation of the membrane, leakage of cytoplasmic content, and eventual cell death. Additionally, flavonoids present in propolis impact topoisomerase-IV activity, leading to growth inhibition of bacterial cells.[64] Although the flavonoids and phenolics present in propolis can sometimes act as antioxidants, the multifaceted antimicrobial mechanism of NO through formation of reactive nitrogen species and rapid and localized NO release shows unobstructed efficacy.[18] The intrinsic antimicrobial ability of propolis when combined with NO contributes towards a complementary antimicrobial response, suggesting that the antioxidant constituents do not fully quench the reactive species formation and antimicrobial pathways of NO. The proposed combination of numerous bacteriolysis pathways of NO and propolis leads to enhanced antimicrobial activity without triggering any adverse toxicity.[68,69]

3.6 Long-term antimicrobial activity

Although the fabricated samples have shown excellent antimicrobial activity in a 24 h bacterial assay, it is important to establish that they are suitable for long-term antibacterial applications to extend the lifetime of medical devices. The samples have shown physiologically relevant levels of NO release for 7 days in addition to a steady release of propolis for 28 days, as shown through propolis leaching *via* UV vis spectrophotometry. To confirm the long-term antibacterial activity of the films, the samples were incubated in PBS at 37 °C for 7, 14, and 28 days before subjecting them to a 24 h antibacterial assay against *S. aureus* as discussed in section 3.5.

The combinatorial propolis and NO releasing samples (5%P–S) incubated for 7 and 14 days in PBS prior to a 24 h antibacterial assay demonstrated a significant reduction in viability of adhered and planktonic *S. aureus*. A >99%

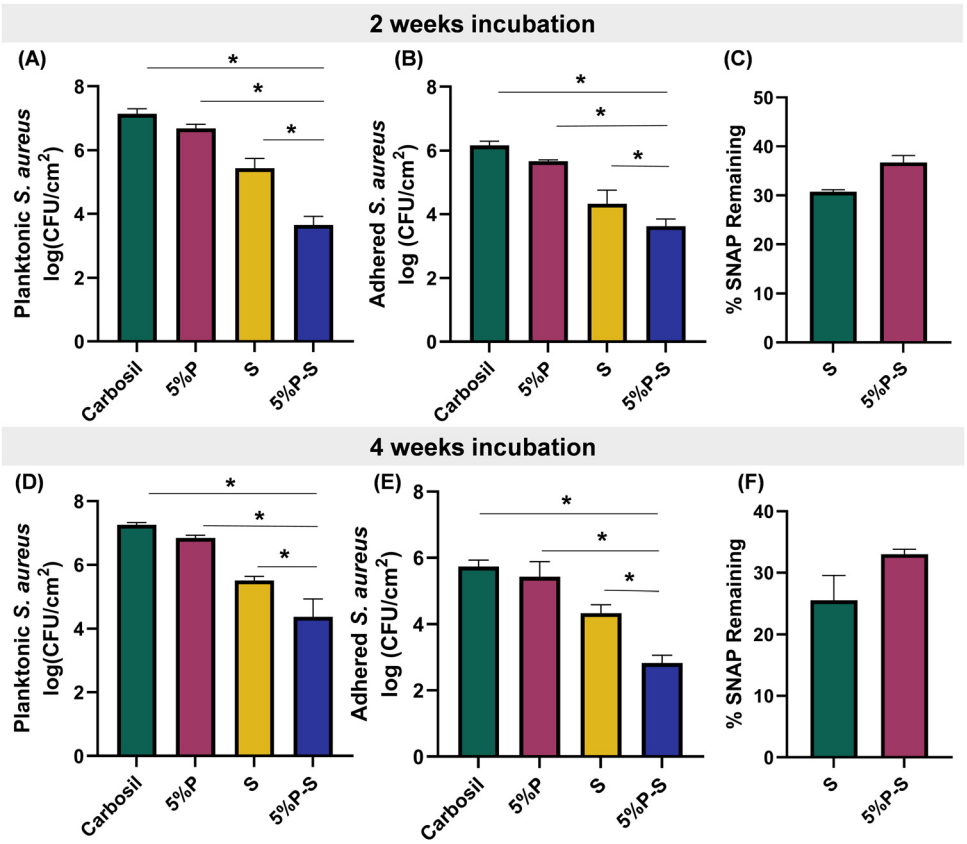

Fig. 4 Reduction in viability of (A) planktonic and (B) adhered *S. aureus* with 5%P–S samples after incubation in physiological conditions for 14 d. (C) Percentage of SNAP remaining in the film samples after 14 d incubation, quantified by UV-vis spectrophotometry. Reduction in viability of (D) planktonic and (E) adhered *S. aureus* with 5%P–S samples after incubation in physiological conditions for 28 d. (F) Percentage of SNAP remaining in the film samples after 28 d incubation, quantified by UV-vis spectrophotometry. Comparisons against control values were performed using one-way ANOVA with Tukey's method. * represents $p \leq 0.05$. All data are presented as mean ± SD ($n \geq 4$).

reduction in viability of adhered *S. aureus* was observed for both incubation periods (7 and 14 d) with the 5%P–S group, as well as >95% reduction in planktonic viability when compared to Carbosil control (Fig. S7 and Fig. 4A and B). When the efficacy of samples incubated for 28 days was exposed to *S. aureus* solution, a similar trend as seen with the fresh samples was observed. A 34.55% reduction was observed with 5%P, whereas an impressive 95.86% and 99.87% reduction in viability of adhered *S. aureus* was observed with S and 5%P–S samples, respectively, when compared to Carbosil control (Fig. 4D). Additionally, 5%P–S samples showed a 99.79% reduction in viability of planktonic *S. aureus* (Fig. 4E). The effectiveness of the samples after incubation under physiological conditions for a week shows that this material has the potential for use in long-term antimicrobial applications. A SNAP loading study comparing the fresh samples with the samples incubated under physiological conditions for 14 and 28 days showed that 30.71% and 36.71% of initially loaded SNAP in S and 5%P–S were still present in the 14 d incubation samples (Fig. 4C). Similarly, 28.52% and 33.06% SNAP were found to be present in S and 5%P–S samples incubated at 37 °C for 14 d (Fig. 4F). These results demonstrate that 5%P–S samples maintain their NO reservoir for up to 28 days and can exert excellent antimicrobial activity when combined with the steady release of propolis.

3.7 Cytocompatibility analysis

With promising antimicrobial results, it is also crucial to establish that the fabricated samples are cytocompatible and would not have any adverse effect on healthy mammalian cells. Here, the cytocompatibility of the fabricated films was tested against NIH 3T3 mouse fibroblast cells. A leachate based MTT assay was performed following the ISO 10993 standard to assess the compatibility of the samples against mammalian cells. Specifically, the MTT assay is based on enzymatic reduction of yellow 3-(4,5-dimethylthiazol-2-yl)-2,5-diphenyl-2*H*-tetrazolium bromide (MTT) to purple formazan in metabolically active cells, which can be quantified through absorbance reading (Fig. 5A).[70] All the tested film samples were found to have a relative cell viability of >90%, which meets the ISO requirement for the biocompatible threshold of 70% (Fig. 5B).[71] Additionally, an indirect contact cytocompatibility test was performed to analyze the compatibility of the fabricated samples against cells in real time. The results from the indirect-contact study also demonstrated no cytotoxic concerns when compared to the cell control (Fig. S8). The results also support

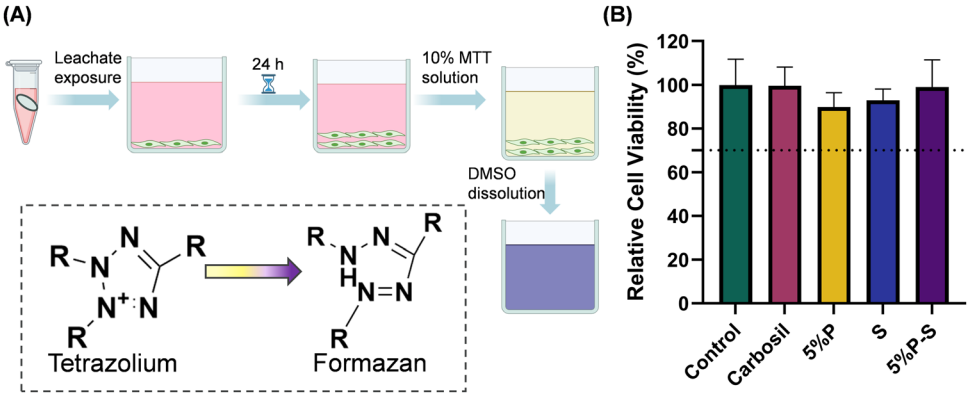

Fig. 5 (A) Schematic of an MTT based cytocompatibility assay that quantifies the ability of metabolically active cells to reduce the yellow tetrazolium salt (MTT) to purple formazan crystals *via* mitochondrial enzymes. (B) Cytocompatibility of the fabricated films as evaluated against 3T3 mouse fibroblast cells through a leachate-based MTT assay. All data are presented as mean ± SD ($n \geq 4$).

the previous cytocompatibility reports of RSNO incorporated polymeric matrices.[72,73] In addition to excellent cytocompatibility, all the tested samples showed <2% hemolytic activity when exposed to porcine blood (Fig. S9). The ability of this material to exert effective antimicrobial activity without eliciting any toxicity concern provides potential for its use in a wide range of medical devices such as catheters and implants.

4. Conclusions

The current work proposes the fabrication of a dual-action NO and propolis releasing polymeric substrate. The fabricated film demonstrated NO release for 7 days with steady propolis release for 28 days to extend the antimicrobial life span of the material. The dual-action antimicrobial film showed excellent antimicrobial efficacy against *S. aureus*, *E. coli*, and *C. albicans* with 99.93%, 97.16%, and 99.69% reduction in viability of adhered bacteria, respectively. Additionally, a significant reduction in the viability of *S. aureus* was observed with 5%P–S films even after incubation under physiological conditions for 28 days, demonstrating the ability of this material to be used in long-term medical device applications following confirmation of long-term antimicrobial activity with other bacterial strains. Future studies should also analyze the interplay between NO and propolis to identify the exact antimicrobial mechanism at play through mechanistic assays. The fabricated samples showed compatibility with fibroblast cells, with >90% relative cell viability for all the fabricated samples. With additional analytical investigation and standardization of propolis, the current technique for the fabrication of a dual-action antimicrobial polymeric matrix can be extended for use in various medical devices such as catheters, vascular ports, implants, *etc.* to demonstrate long-term antibacterial and antifungal activity without contributing towards AMR.

Conflicts of interest

The authors declare the following competing financial interest(s): Hitesh Handa and Elizabeth J. Brisbois are the co-founders and maintain a financial interest in a startup company investigating nitric oxide as a biomedical therapeutic for medical devices.

Data availability

The data supporting this article have been included as part of the supplementary information (SI). Supplementary information: UV-vis spectra of propolis with different concentrations; calibration curve of propolis at 275 nm; UV-vis spectra of SNAP with different concentrations; calibration curve of SNAP at 340 nm; ^{1}H NMR spectrum of NAP in DMSO-d6; ^{1}H NMR spectrum of SNAP in DMSO-d6; antibacterial assay against *S. aureus* after 7 d of storage under physiological conditions; cytocompatibility of the samples tested with 3T3 mouse fibroblast cells through indirect contact MTT assay. See DOI: https://doi.org/10.1039/d6tb00666c.

Acknowledgements

We thank Isabel Martinez for her assistance with the hemolysis study. This work was supported by the National Institute of Health through funds received under NIH R01HL172496. Graphics were created by the authors using the BioRender.com software.

References

1 R. M. Klevens, J. R. Edwards, C. L. Richards, T. C. Horan, R. P. Gaynes, D. A. Pollock and D. M. Cardo, *Public Health Rep.*, 2007, **122**, 160–166.
2 D. S. Yokoe, S. D. Advani, D. J. Anderson, H. M. Babcock, M. Bell, S. M. Berenholtz, K. A. Bryant, N. Buetti, M. S. Calderwood, D. P. Calfee, V. M. Deloney, E. R. Dubberke, K. D. Ellingson, N. O. Fishman, D. N. Gerding, J. Glowicz, M. K. Hayden, K. S. Kaye, L. K. Kociolek, E. Landon, E. L. Larson, A. N. Malani, J. Marschall, J. Meddings, L. A. Mermel, P. K. Patel, T. M. Perl, K. J. Popovich, J. K. Schaffzin, E. Septimus, K. K. Trivedi, R. A. Weinstein

and L. L. Maragakis, *Infect. Control Hosp. Epidemiol.*, 2023, **44**, 1533–1539.
3 F. Prestinaci, P. Pezzotti and A. Pantosti, *Pathog. Global Health*, 2015, **109**, 309–318.
4 S. M. H. Richmond, *Rev. Infect. Dis.*, 1988, **10**, 677.
5 R. Laxminarayan, A. Duse, C. Wattal, A. K. M. Zaidi, H. F. L. Wertheim, N. Sumpradit, E. Vlieghe, G. L. Hara, I. M. Gould, H. Goossens, C. Greko, A. D. So, M. Bigdeli, G. Tomson, W. Woodhouse, E. Ombaka, A. Q. Peralta, F. N. Qamar, F. Mir, S. Kariuki, Z. A. Bhutta, A. Coates, R. Bergstrom, G. D. Wright, E. D. Brown and O. Cars, *Lancet Infect. Dis.*, 2013, **13**, 1057–1098.
6 K. E. Fleming-Dutra, A. L. Hersh, D. J. Shapiro, M. Bartoces, E. A. Enns, T. M. File, J. A. Finkelstein, J. S. Gerber, D. Y. Hyun, J. A. Linder, R. Lynfield, D. J. Margolis, L. S. May, D. Merenstein, J. P. Metlay, J. G. Newland, J. F. Piccirillo, R. M. Roberts, G. V. Sanchez, K. J. Suda, A. Thomas, T. M. Woo, R. M. Zetts and L. A. Hicks, *JAMA*, 2016, **315**, 1864.
7 T. P. Van Boeckel, C. Brower, M. Gilbert, B. T. Grenfell, S. A. Levin, T. P. Robinson, A. Teillant and R. Laxminarayan, *Proc. Natl. Acad. Sci. U. S. A.*, 2015, **112**, 5649–5654.
8 M. García-Castro, F. Sarabia, A. Díaz-Morilla and J. M. López-Romero, *Explor. Drug Sci.*, 2023, **1**, 180–209.
9 V. M. Rocha, R. D. Portela, J. P. Dos Anjos, C. O. De Souza and M. A. Umsza-Guez, *Food Prod., Process. Nutr.*, 2023, 5.
10 S. I. Anjum, A. Ullah, K. A. Khan, M. Attaullah, H. Khan, H. Ali, M. A. Bashir, M. Tahir, M. J. Ansari, H. A. Ghramh, N. Adgaba and C. K. Dash, *Saudi J. Biol. Sci.*, 2019, **26**, 1695–1703.
11 E. Rojczyk, A. Klama-Baryła, W. Łabuś, K. Wilemska-Kucharzewska and M. Kucharzewski, *J. Ethnopharmacol.*, 2020, **262**, 113159.
12 S. Castaldo and F. Capasso, *Fitoterapia*, 2002, **73**, S1–S6.
13 P. K. Patel, A. Gupta, V. M. Vaughn, J. D. Mann, J. M. Ameling and J. Meddings, *J. Hosp. Med.*, 2018, **13**, 105–116.
14 K. Kainz, M. A. Bauer, F. Madeo and D. Carmona-Gutierrez, *Microb. Cell*, 2020, **7**, 143–145.
15 B. N. Gantner, K. M. LaFond and M. G. Bonini, *Redox Biol.*, 2020, **34**, 101550.
16 M. W. Vaughn, L. Kuo and J. C. Liao, *Am. J. Physiol.: Heart Circ. Physiol.*, 1998, **274**, H2163–H2176.
17 U. Forstermann and W. C. Sessa, *Eur. Heart J.*, 2012, **33**, 829–837.
18 D. O. Schairer, J. S. Chouake, J. D. Nosanchuk and A. J. Friedman, *Virulence*, 2012, **3**, 271–279.
19 L. M. Estes Bright, M. R. S. Garren, M. Ashcraft, A. Kumar, H. Husain, E. J. Brisbois and H. Handa, *ACS Appl. Mater. Interfaces*, 2022, **14**, 21916–21930.
20 H. Massoumi, R. Kumar, M. K. Chug, Y. Qian and E. J. Brisbois, *ACS Appl. Bio Mater.*, 2022, **5**, 2285–2295.
21 E. J. Brisbois, H. Handa, T. C. Major, R. H. Bartlett and M. E. Meyerhoff, *Biomaterials*, 2013, **34**, 6957–6966.
22 A. Sapkota, A. Mondal, M. K. Chug and E. J. Brisbois, *J. Biomed. Mater. Res., Part A*, 2023, **111**, 1627–1641.
23 M. K. Chug, A. Sapkota, M. Garren and E. J. Brisbois, *J. Controlled Release*, 2024, **375**, 667–680.
24 M. J. Goudie, J. Pant and H. Handa, *Sci. Rep.*, 2017, **7**, 13623.
25 D. A. Riccio and M. H. Schoenfisch, *Chem. Soc. Rev.*, 2012, **41**, 3731.
26 M. K. Chug and E. J. Brisbois, *ACS Mater. Au*, 2022, **2**, 525–551.
27 T.-K. Nguyen, R. Selvanayagam, K. K. K. Ho, R. Chen, S. K. Kutty, S. A. Rice, N. Kumar, N. Barraud, H. T. T. Duong and C. Boyer, *Chem. Sci.*, 2016, **7**, 1016–1027.
28 K. R. Rouillard, O. P. Novak, A. M. Pistiolis, L. Yang, M. J. R. Ahonen, R. A. McDonald and M. H. Schoenfisch, *ACS Infect. Dis.*, 2021, **7**, 23–33.
29 I. Chipinda and R. H. Simoyi, *J. Phys. Chem. B*, 2006, **110**, 5052–5061.
30 Y. Wo, E. J. Brisbois, R. H. Bartlett and M. E. Meyerhoff, *Biomater. Sci.*, 2016, **4**, 1161–1183.
31 E. J. Brisbois, T. C. Major, M. J. Goudie, R. H. Bartlett, M. E. Meyerhoff and H. Handa, *Acta Biomater.*, 2016, **37**, 111–119.
32 S. Altabbal, K. Athamnah, A. Rahma, A. F. Wali, A. H. Eid, R. Iratni and Y. Al Dhaheri, *Pharmaceuticals*, 2023, **16**, 450.
33 P. P. Wieczorek, N. Hudz, O. Yezerska, V. Horčinová-Sedláčková, M. Shanaida, O. Korytniuk and I. Jasicka-Misiak, *Molecules*, 2022, **27**, 1600.
34 L. S. Contieri, L. M. de Souza Mesquita, V. L. Sanches, J. Viganó, J. Martinez, D. T. da Cunha and M. A. Rostagno, *Food Res. Int.*, 2022, **161**, 111846.
35 T. Sato, D. Mello, L. Vasconcellos, A. Valente and A. Borges, *Int. J. Mol. Sci.*, 2020, **21**, 4561.
36 M. El-Sakhawy, A. Salama and S. A. A. Mohamed, *Biomass Convers. Biorefin.*, 2024, **14**, 13731–13746.
37 Y. Wo, Z. Li, E. J. Brisbois, A. Colletta, J. Wu, T. C. Major, C. Xi, R. H. Bartlett, A. J. Matzger and M. E. Meyerhoff, *ACS Appl. Mater. Interfaces*, 2015, **7**, 22218–22227.
38 A. Mondal, P. Maffe, S. N. Wilson, S. Ghalei, R. Palacio, H. Handa and E. J. Brisbois, *Mater. Adv.*, 2023, **4**, 3197–3206.
39 S. H. Lee, S. Yoo, S. H. Kim, Y. M. Kim, S. I. Han and H. Lee, *Mater. Today Bio*, 2025, **31**, 101615.
40 T. A. Tabish, N. D. Thorat and R. J. Narayan, *Mech. Mater.*, 2023, **176**, 104520.
41 Y. Wo, Z. Li, A. Colletta, J. Wu, C. Xi, A. J. Matzger, E. J. Brisbois, R. H. Bartlett and M. E. Meyerhoff, *Composites, Part B*, 2017, **121**, 23–33.
42 N. T. Linh, K. H. Lee and B. T. Lee, *J. Biomed. Mater. Res., Part A*, 2013, **101**, 2412–2423.
43 S. Y. Chew, T. C. Hufnagel, C. T. Lim and K. W. Leong, *Nanotechnology*, 2006, **17**, 3880–3891.
44 Y. Wo, Z. Li, A. Colletta, J. Wu, C. Xi, A. J. Matzger, E. J. Brisbois, R. H. Bartlett and M. E. Meyerhoff, *Composites, Part B*, 2017, **121**, 23–33.
45 M. Goudie, E. Brisbois, A. Thompson, J. Potkay and H. Handa, *Int. J. Polym. Mater. Polym. Biomater.*, 2016, **65**, 769–778.
46 Y. Wo, Z. Li, E. J. Brisbois, A. Colletta, J. Wu, T. C. Major, C. Xi, R. H. Bartlett, A. J. Matzger and M. E. Meyerhoff, *ACS Appl. Mater. Interfaces*, 2015, **7**, 22218–22227.
47 K. A. Broniowska, A. R. Diers and N. Hogg, *Biochim. Biophys. Acta, Gen. Subj.*, 2013, **1830**, 3173–3181.

48 T. C. Major, D. O. Brant, C. P. Burney, K. A. Amoako, G. M. Annich, M. E. Meyerhoff, H. Handa and R. H. Bartlett, *Biomaterials*, 2011, **32**, 5957–5969.
49 L. M. Estes Bright, Y. Wu, E. J. Brisbois and H. Handa, *Curr. Opin. Colloid Interface Sci.*, 2023, **66**, 101704.
50 M. Ganzarolli De Oliveira, *Basic Clin. Pharmacol. Toxicol.*, 2016, **119**, 49–56.
51 L. Yang, L. Jing, Y. Jiao, L. Wang, J. T. Marchesan, S. Offenbacher and M. H. Schoenfisch, *Mol. Pharmaceutics*, 2019, **16**, 4017–4023.
52 T. Yang, A. N. Zelikin and R. Chandrawati, *Adv. Sci.*, 2018, **5**, 1701043.
53 R. J. Singh, N. Hogg, J. Joseph and B. Kalyanaraman, *J. Biol. Chem.*, 1996, **271**, 18596–18603.
54 D. T. Nguyen, J. Pant, A. Sapkota, M. J. Goudie, P. Singha, E. J. Brisbois and H. Handa, *J. Biomed. Mater. Res., Part A*, 2024, **112**, 1930–1940.
55 T. N. Hiew, D. L. H. Tan, Y. L. Tiang and P. W. S. Heng, *Int. J. Pharm.*, 2019, **557**, 229–237.
56 A. Mondal, M. Douglass, S. P. Hopkins, P. Singha, M. Tran, H. Handa and E. J. Brisbois, *ACS Appl. Mater. Interfaces*, 2019, **11**, 34652–34662.
57 L. C. Pamplona-Zomenhan, B. C. Pamplona, C. B. D. Silva, M. C. Marcucci and L. M. J. Mimica, *Braz. J. Microbiol.*, 2011, **42**, 1259–1264.
58 K. Grecka, Z. R. Xiong, H. Chen, K. Pełka, R. W. Worobo and P. Szweda, *Pathogens*, 2020, **9**, 646.
59 C. J. Crnich and D. G. Maki, *Clin. Infect. Dis.*, 2002, **34**, 1232–1242.
60 J. S. Ogeer-Gyles, K. A. Mathews and P. Boerlin, *J. Vet. Emerg. Crit. Care*, 2006, **16**, 1–18.
61 F. C. Fang, *mBio*, 2011, **2**, e00141-11.
62 N. Rivera-Yañez, C. R. Rivera-Yañez, G. Pozo-Molina, C. F. Méndez-Catalá, J. Reyes-Reali, M. I. Mendoza-Ramos, A. R. Méndez-Cruz and O. Nieto-Yañez, *Biology*, 2021, **10**, 428.
63 A. Sapkota, A. Mondal, M. K. Chug and E. J. Brisbois, *J. Biomed. Mater. Res., Part A*, 2023, **111**, 1627–1641.
64 M. S. Almuhayawi, *Saudi J. Biol. Sci.*, 2020, **27**, 3079–3086.
65 E. M. Hetrick, J. H. Shin, N. A. Stasko, C. B. Johnson, D. A. Wespe, E. Holmuhamedov and M. H. Schoenfisch, *ACS Nano*, 2008, **2**, 235–246.
66 L. Piacenza, A. Zeida, M. Trujillo and R. Radi, *Physiol. Rev.*, 2022, **102**, 1881–1906.
67 T. C. Harrop, Z. J. Tonzetich, E. Reisner and S. J. Lippard, *J. Am. Chem. Soc.*, 2008, **130**, 15602–15610.
68 L. Yang, E. S. Feura, M. J. R. Ahonen and M. H. Schoenfisch, *Adv. Healthcare Mater.*, 2018, **7**, 1800155.
69 S. Touzani, W. Embaslat, H. Imtara, A. Kmail, S. Kadan, H. Zaid, I. Elarabi, L. Badiaa and B. Saad, *BioMed Res. Int.*, 2019, **2019**, 1–11.
70 B. Huzum, B. Puha, R. Necoara, S. Gheorghevici, G. Puha, A. Filip, P. Sirbu and O. Alexa, *Exp. Ther. Med.*, 2021, **22**, 1315.
71 W. H. De Jong, J. W. Carraway, C. Liu, C. Fan, J. Liu, A. P. Turley, T. S. Rollins and K. P. Coleman, *Toxicol. In Vitro*, 2020, **69**, 104995.
72 M. K. Chug and E. J. Brisbois, *J. Controlled Release*, 2022, **349**, 227–240.
73 S. Ghalei, M. Douglass and H. Handa, *ACS Biomater. Sci. Eng.*, 2022, **8**, 273–283.